Materials and Design 160 (2018) 325–337

Contents lists available at ScienceDirect

Materials and Design

journal homepage: www.elsevier.com/locate/matdes

Axial compressive collapse of ultralight corrugated sandwich cylindrical shells

Peng-Bo Su [a,b], Bin Han [c,d,e,*], Mao Yang [a,b], Zi-Han Wei [a,b], Zhen-Yu Zhao [a,b], Qian-Cheng Zhang [a,g], Qi Zhang [c], Ke-Ke Qin [f], Tian Jian Lu [b,g,**]

[a] State Key Laboratory for Strength and Vibration of Mechanical Structures, Xi'an Jiaotong University, Xi'an 710049, PR China
[b] State Key Laboratory of Mechanics and Control of Mechanical Structures, Nanjing University of Aeronautics and Astronautics, Nanjing 210016, PR China
[c] School of Mechanical Engineering, Xi'an Jiaotong University, Xi'an 710049, PR China
[d] School of Engineering, Brown University, Providence, RI 02912, USA
[e] Research institute of Xi'an Jiaotong University, Zhejiang, Hangzhou 311212, PR China
[f] Beijing Electro-Mechanical Engineering Institute, Beijing 10074, PR China
[g] MOE Key Laboratory for Multifunctional Materials and Structures, Xi'an Jiaotong University, Xi'an 710049, PR China

HIGHLIGHTS

- Novel all-metallic sandwich cylindrical shells with corrugated cores are proposed.
- Quasi-static axial compressive behavior including initial collapse and folding deformation is studied.
- The superiority of sandwich shells over monolithic shells in terms of initial failure load and energy absorption is dramatic.

GRAPHICAL ABSTRACT

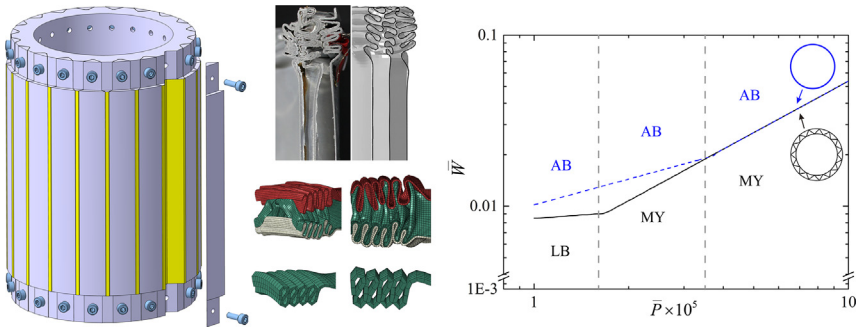

ARTICLE INFO

Article history:
Received 20 July 2018
Received in revised form 1 September 2018
Accepted 17 September 2018
Available online 18 September 2018

Keywords:
Sandwich cylindrical shell
Corrugated core
Axial compression
Minimum weight design

ABSTRACT

Ultralight all-metallic sandwich cylindrical shells with corrugated cores are designed and fabricated using a method involving tamping and shape correction. Quasi-static axial compressive behaviors of the sandwich shells are investigated using a combined experimental, theoretical and numerical approach. Based on the analytical model and numerical approach, systematic parametric study is carried out to explore the effects of key geometrical parameters on the failure load and energy absorption capacity. Minimum weight design as a function of the failure load is subsequently carried out for the proposed sandwich shell. As an attempt for further performance enhancement, the foam-filled corrugated-core sandwich cylindrical shell is proposed and a preliminary experimental study is carried out. The superiority of sandwich shells over monolithic shells in terms of initial failure load and energy absorption is clearly demonstrated, potentially important for applications demanding simultaneous ultra-lightweight, load-bearing and energy absorption.

* Correspondence to: B. Han, School of Mechanical Engineering, Xi'an Jiaotong University, Xi'an 710049, PR China.
** Correspondence to: T.J. Lu, State Key Laboratory of Mechanics and Control of Mechanical Structures, Nanjing University of Aeronautics and Astronautics, Nanjing 210016, PR China.
E-mail addresses: hanbinghost@mail.xjtu.edu.cn (B. Han), tjlu@nuaa.edu.cn (T.J. Lu).

https://doi.org/10.1016/j.matdes.2018.09.034

Nomenclature

R_o	radius of outer facesheet (mm)
R_i	radius of inner facesheet (mm)
h	core height (mm)
l	corrugated plate length (mm)
f	width of corrugation platform (mm)
α	corrugation angle (deg)
t_c	corrugated core thickness (mm)
t_f.	facesheet thickness (mm)
H	axial length of the cylindrical shell (mm)
N	number of corrugated units in the core
W	the mass per length of the structure (kg/mm)
P_{EB}	Euler buckling load (kN)
P_{AB}	axisymmetric buckling load (kN)
P_{SB}	shell buckling load (kN)
P_{MY}	material yielding load (kN)
ε	compressive strain of the sandwich cylinder
E	energy absorption (kJ)
w	maximal deflection perpendicular to corrugation webs (mm)
$\overline{t}_f$	non-dimensional facesheet thickness
$\overline{t}_c$	non-dimensional core thickness
$\overline{h}$	non-dimensional core height
$\overline{H}$	non-dimensional axial length of the cylindrical shell
$\overline{W}$	non-dimensional mass per length
$\overline{P}$	non-dimensional axial compression load
N	number of corrugated units in the core

1. Introduction

Cylindrical shells are widely used in aeronautical and astronautical applications, such as the interstages of launch vehicles and the fuselage sections of civil/military aircrafts. These structures, including monolithic, stiffened and sandwich shells, are often subjected to axial compressive loading. Early researches concerning sandwich cylindrical shells mainly focused on sandwich wall structures with foam and honeycomb cores to demonstrate the superiority of these structures in weight savings. For instance, Agarwal and Sobelt [1] conducted optimization studies for stiffened, unstiffened, and sandwich cylindrical shells and found sandwich shells with graphite/epoxy faces and aluminum honeycomb cores are most weight effective over a wide range of external loads. Also, Hutchinson and He [2] investigated the buckling of metal foam filled sandwich cylindrical shells and undertook optimization analysis for such structures. They found that sandwich cylindrical shells have a competitive weight advantage over stringer stiffened counterparts. Additional studies on the axial compressive performance of foam/honeycomb core sandwich cylindrical shells can be found in Refs. [3–8].

It has been demonstrated that, compared with foam/honeycomb core sandwich panels, sandwich panels with three-dimensional (3D) truss or two-dimensional (2D) prismatic cores offer equal or greater weight savings and design advantages [9–11]. Especially corrugated sandwich constructions, these structures have open core topologies and can be designed as integral thermal protection system to provide thermal protection and load capabilities for outer covering of manned spacecrafts [12]. Meanwhile, the development of novel composite materials [13,14] has provided a greater flexibility in fabrication and multifunctional applications of sandwich panels, such as carbon fiber reinforced composite honeycombs [15], 3D integrated core sandwich composites [16], hybrid lightweight composite pyramidal truss sandwich panels [17], and carbon fiber reinforced silicon carbide corrugated core sandwich structures [18], etc.

Inspired by these studies, composite sandwich cylindrical shells with such truss and prismatic cores have been investigated. The technique of hot press moulding was successfully used to fabricate sandwich cylindrical shells with several kinds of truss and prismatic cores. Xiong et al. [19] manufactured the sandwich cylindrical shells with aluminum pyramidal truss cores and carbon fiber facesheets. They also fabricated the corrugated sandwich cylinder with carbon fiber reinforced composites and conducted the compression tests [20]. A relevant large scale corrugated core sandwich cylinder with carbon fiber reinforced composites was designed and made by Li et al. [21], in which the strength and failure mode is studied. Yang et al. [22] manufactured the same corrugated sandwich structure and studied the vibration and damping characteristics of such structures. Furthermore, Yang et al. [23] designed and fabricated sandwich cylindrical shells with pyramidal truss-like cores with carbon fiber reinforced composites, and studied the modal response. Alternatively, apart from the hot press moulding, composite sandwich cylindrical shells were also designed and fabricated with filament winding and twice co-curing processes. Fan et al. [24] proposed the carbon fiber reinforced composite (CFRC) sandwich cylinder with Kagome cores. They revealed the stiffness and load capacity of the fabricated structure under axial compression. Based on this work, there were several studies concerned with the stiffness, strength and modal response of composite lattice core sandwich cylinder [25–30].

At present, truss/prismatic core sandwich cylindrical shells are mainly fabricated using fiber-reinforced composite materials. Compared with the composite materials, metals have the advantage of high toughness, low cost and deforming largely in plastic stage, leading to synergistic benefits in strength and energy absorption. Nonetheless, there exists rare systematic theoretical and experimental study on the buckling and collapse behaviors of all-metallic sandwich cylindrical shells with either 3D truss or 2D prismatic cores, except for the studies of Zhang et al. [31,32] and Liu et al. [33]. Zhang et al. [31,32] investigated the energy absorption capacity of aluminum Kagome honeycomb sandwich cylindrical columns and compared these structures with aluminum foam-filled cylindrical columns under axial crushing loads. Their work was nonetheless only carried out with finite element method, without fabrication and testing of the sandwich structure. Liu et al. [33] fabricated a kind of metallic sandwich shell with star-shaped tube core using the technique of wire-cut electrical discharge machining (WEDM) and investigated the crushing behavior of such structure. However, these authors did not bond the star-shaped core with the facesheets and did not investigate the strength as well as failure modes of the sandwich tube.

In contrast, we propose in the current study a novel all-metallic corrugated-core sandwich cylindrical shell. Compared with the sandwich shell of Liu et al. [33], we design a relative thin wall structure (thinnest metallic wall of 0.1 mm in the current study relative to 1.2 mm metallic walls in [33]) and more corrugated units in the core (20 units in this paper versus 6 units in [33]). Further, all the components are bonded using high strength epoxy adhesive, which differs greatly in crushing behavior in comparison with that reported by Liu et al. [33]. The mechanism operating in the regime of large deformation in our work is also quite different from that of Liu et al. [33]. Finally, we plan to explore the initial failure load and failure modes for the proposed structure, which is not covered in [33]. In this work, the fabrication, experimental testing, analytical modeling and numerical analysis of this structure are presented, which is organized as follows: details of fabrication and testing are presented in Section 2, analytical modeling of initial failure modes are presented in Section 3, finite element simulations are detailed in Section 4, followed by results and discussions in Section 5 and conclusions in Section 6.

2. Experiment

2.1. Fabrication methodology

With reference to Figs. 1 and 2, an all-metallic sandwich cylindrical shell consisting of two circular facesheets and a circular corrugated

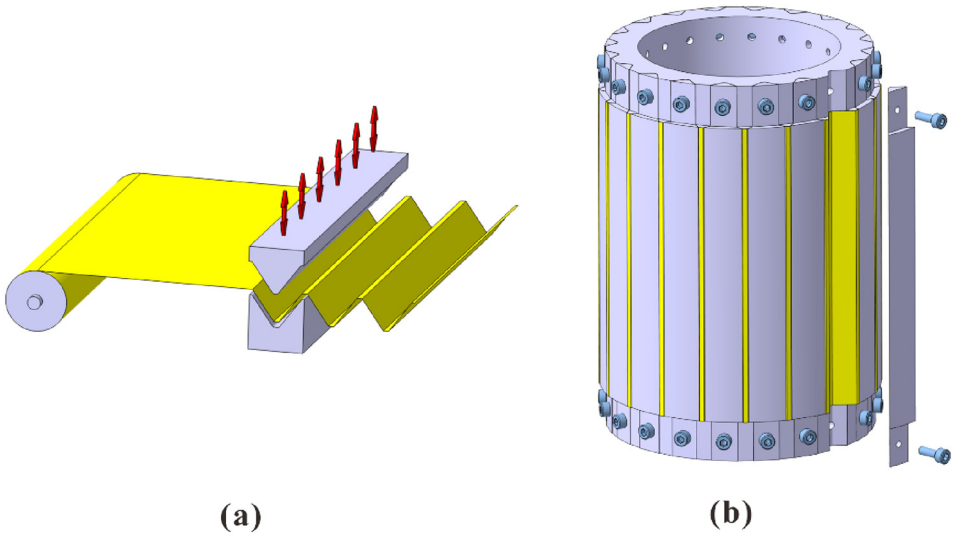

Fig. 1. Schematic of the fabrication process for the corrugated-core sandwich cylindrical shell.

core is fabricated using a two-step process. In the first step, corrugated plate is processed via stamping (Fig. 1a). In the second step, a pair of molds involving a steel cylinder with annular grooves and 20 steel trapezoidal prismatic bars are used to process the curved corrugated core (Fig. 1b). This is essentially a shape correction step, wherein the corrugated plate is inserted into the grooves and bonded in two ends using epoxy adhesive (LOCTITE Hysol E-120HP). Meanwhile, the curved core is fixed by trapezoidal prismatic bars to correct the shape as depicted in Fig. 1b. Subsequently, the prismatic bars are removed and the circular corrugated core is obtained upon demolding. Finally, the inner and outer facesheets are fabricated and assembled with the circular corrugated core. For all of the sandwich components, 1060Al is selected for its convenience in machining quality and high ductility (Fig. 2). Fig. 3 displays the measured tensile stress versus strain curve of 1060Al as well as its elastic-ideally plastic representation.

The critical geometric parameters of the corrugated sandwich cylindrical shell as indicated in Fig. 2. The mass per length of the sandwich cylindrical shell can be defined as:

$$W = 2[(f + l)N + \pi(R_o + R_i)]\rho \tag{1}$$

The mass of the platforms in corrugated cores is less than 5% of the total mass, so the influence of platforms can be neglected. The expression of the mass per length of the structure is further simplified for the convenience of subsequent theoretical analysis, which can be written as:

$$W = 2\pi\rho(2h_c t_f + 4R_i t_f + 2R_i t_c \sec\alpha) \tag{2}$$

A series of corrugated sandwich cylindrical shells with different shell thickness are produced. Relevant physical and geometric parameters of the test samples are listed in Table 1. In addition, all the samples have fixed number of corrugated units in the core (20), fixed inclination angle of corrugated core ($\alpha = 45^{\circ}$), fixed height ($H = 145$ mm), fixed radius of outer facesheet ($R_o = 67.5$ mm) and inner facesheet ($R_i = 57$ mm). As shown in Table 1, two groups of test samples are fabricated, referred to below as S1 and S2, with each group containing 2 identical samples (#1 and #2) so as to check the reproducibility of the experiments. Thus, a total of 4 corrugated-core sandwich cylindrical shell samples are fabricated and tested in the current study.

2.2. Experimental setup

Quasi-static axial compression tests are carried out with a hydraulic testing machine (MTS). Both ends of the sandwich cylindrical shell are clamped with a pair of steel flange plates, as shown in Fig. 4. The lower plate is fixed, while the upper load platen exerts displacement loading with fixed displacement rate of 1 mm/min. A computer-based data acquisition system is employed to record the load and displacement during the compression tests.

To verify the reproducibility of the experiments, two identical samples (#1 and #2) are tested for each group, i.e., sandwich S1 and S2. The sample labelled as #1 is compressed to densification while the other labelled as #2 is compressed to 35%, as to explore the detailed deformation mechanisms during axial compression.

3. Theoretical analysis

3.1. Theoretical model

In this section, simple theoretical analysis is carried out to predict the initial failure load of corrugated-cored sandwich cylindrical shells. Four main failure modes are identified: (1) Euler buckling (EB), (2) axisymmetric buckling (AB), (3) local buckling (LB) and (4) material yielding (MY). The actual initial failure load is dictated by the failure mode associated with the lowest applied load. In the theoretical analysis, it is assumed that the sandwich cylindrical shell is made from an ideal elastic-plastic solid having a Young modulus of 70 GPa and a yielding strength of 140 MPa, respectively (Fig. 3).

3.1.1. Euler buckling

For this type of failure mode, the sandwich cylindrical shell is regarded as a solid thin-wall cylindrical shell with equivalent modulus and thickness [19]. The Euler buckling load of the shell can thence be given as:

$$P_{EB} = \frac{k^2\pi^2(EI)_{eq}}{L^2} \tag{3}$$

in which the value of k is assumed to be 2, corresponding to the boundary condition of fixed ends, and $(EI)_{eq}$ is:

$$(EI)_{eq} = \frac{E\pi(2t_f + t_c\sec\alpha)\left((R_i + h + 2t_f)^4 - R_i^4\right)}{4(2t_f + h)} \tag{4}$$

3.1.2. Axisymmetric buckling

For this type of failure mode, the sandwich cylindrical shell is also assumed as a solid thin-wall cylindrical shell with equivalent modulus

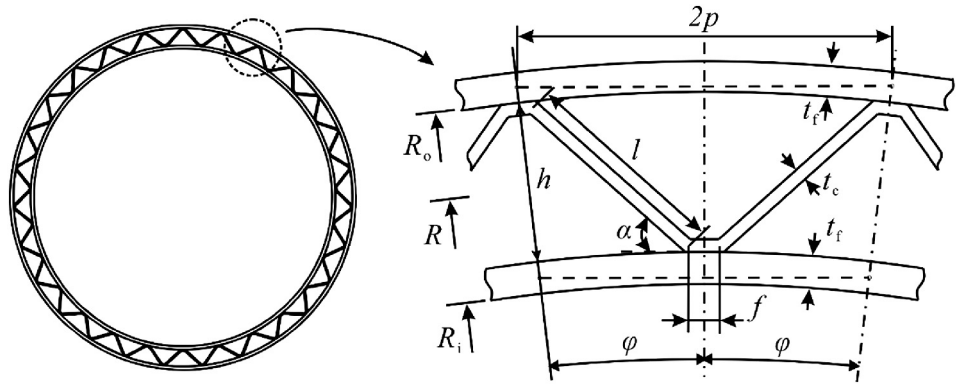

Fig. 2. Geometric parameters of the corrugated-core sandwich cylindrical shell.

and thickness. When axisymmetric buckling of the shell occurs under axial compression, the buckling load per unit area is given by [34]:

$$\sigma_{AB} = \frac{E_{eq}(h + 2t_f)}{R\sqrt{3(1-\nu^2)}} \tag{5}$$

Correspondingly, the failure load of axisymmetric buckling is:

$$P_{AB} = \pi\sigma_{AB}\left((R_i + h + 2t_f)^2 - R_i^2\right) \tag{6}$$

3.1.3. Local buckling

The core webs and facesheets between the two supports of the corrugated core may fail in local buckling under axial compression. The facesheet between two adjacent platforms can be taken as an arch board with small central angle so that, when subjected to compression, it can be assumed as a straight plate according to Timoshenko [34]. Simple support is assumed for the four sides of the facesheet between the two adjacent platforms and the core web. This assumption results in a conservative failure load. Under such conditions, the local buckling load per unit area can be obtained as [34]:

$$\sigma_{LB} = \begin{cases} \dfrac{\pi^2 E}{3(1-\nu^2)}\left(\dfrac{t_f}{2p}\right)^2 & \dfrac{t_f}{t_c} \le 2\cos\alpha, \text{ face sheet buckling} \\ \dfrac{\pi^2 E}{3(1-\nu^2)}\left(\dfrac{t_c}{l}\right)^2 & \dfrac{t_f}{t_c} > 2\cos\alpha, \text{ core web buckling} \end{cases} \tag{7}$$

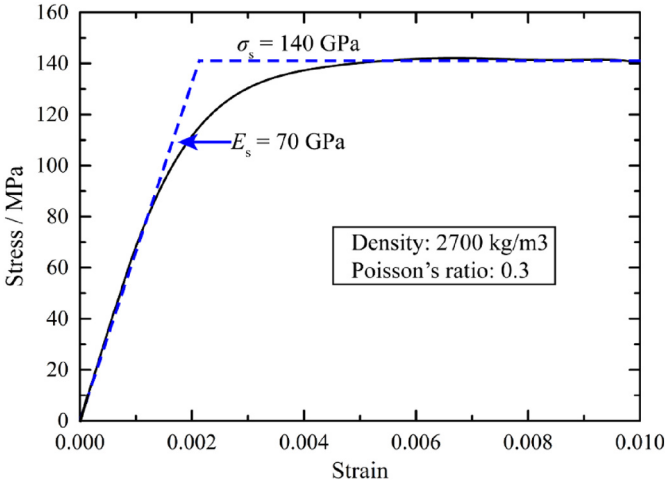

Fig. 3. Measured tensile stress versus strain curve for 1060Al (solid line) and elastic-ideally plastic representation (dash line).

where $p = l\cos\alpha$ according to Fig. 2. Correspondingly, the critical load of local buckling is:

$$P_{LB} = 2\pi\sigma_{LB}(h_c t_f + 2R_i t_f + R_i t_c \sec\alpha) \tag{8}$$

3.1.4. Material yielding

Material yielding of both the corrugated core and the facesheets is taken into account. The corresponding critical load can be expressed as:

$$P_{MY} = 2\pi\sigma_Y(h_c t_f + 2R_i t_f + R_i t_c \sec\alpha) \tag{9}$$

3.2. Failure maps

To identify the dominant initial failure modes of a corrugated-core sandwich cylindrical shell, failure maps are constructed using the formulas presented in the previous section, with fixed corrugation angle ($\alpha = 45^\circ$) and fixed $L/R_o = 2.18$. The dependence of t_f/R_o and h/R_o on dominant initial failure modes is explored. Meanwhile, the influence of t_c/t_f on dominant initial failure modes is quantified. As shown in Fig. 5, for the sandwich cylindrical shell with corrugated core, the dominant initial failure modes are local buckling (LB), material yielding (MY) and axisymmetric buckling (AB).

Notice that Euler buckling has been taken into consideration when we construct the failure map in Fig. 5. Nonetheless, even though we define a considerable range of variables in order to display more failure modes, Euler buckling does not occur and hence is absent in Fig. 5. It should be noted that, limited to the manufacturing technology in laboratory, both S1 and S2 employed in the present study only fail in local buckling in the circular corrugated core (Fig. 5).

4. Finite element modeling

Finite element (FE) simulations of sandwich cylindrical shells under quasi-static axial compression are carried out with ABAQUS/Explicit. The geometric parameters are identical to those of the experimental specimens, and two rigid plates are used to model the puncher. The small geometric imperfections induced during fabrication process is

Table 1
Physical and geometrical parameters of corrugated-core sandwich cylindrical shell samples.

Samples	t_f (mm)	t_c (mm)	Total mass (g)	Mass of Al (g)	Mass of epoxy resign (g)
S1	0.2	0.1	93.15	86.04	7.11
			91.82	85.59	6.23
S2	0.4	0.2	177.3	171.76	5.54
			175.75	171.84	3.91

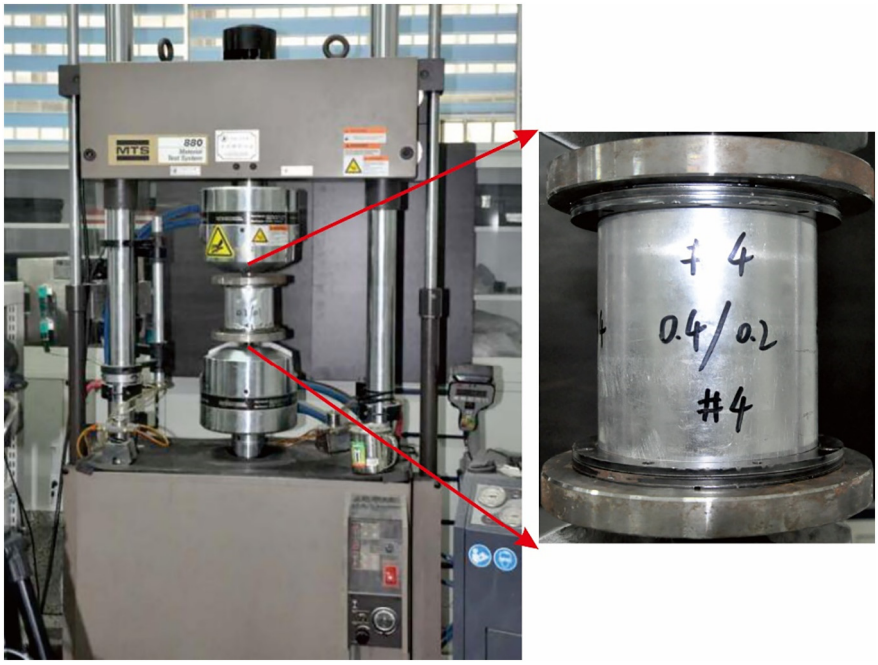

Fig. 4. Test set up of axial compression.

ignored. Four-node shell elements (S4R) with five integration points through the thickness are used to model the facesheets and corrugated core, with the size of 1 mm × 1 mm. Four-node rigid elements (R3D4) are employed to model the puncher, with the size of 2 mm × 2 mm. Mesh sensitivity study shows that further mesh refining does not improve the accuracy of FE simulation (results not shown here for brevity).

General contact is employed for all the models with the Coulomb friction coefficient fixed at 0.2. Interfaces between the core and the facesheets are treated as perfectly bonded. Axial loading is applied by the top rigid plate moving at a sufficiently slow speed to mimic quasi-static loading. This quasi-static loading procedure is verified (results not shown for brevity) according to the principles proposed by Santosa et al. [35]: the total kinetic energy must be very small compared to the total internal energy over the period of the crushing process and the crushing force-displacement response should be independent from the applied velocity.

Both the facesheets and the corrugated core are made of 1060Al (ρ_s = 2700 kg/m^3), which is modeled as an isotropic elastic–plastic solid governed by the von Mises J2 flow theory. The Young's modulus and Poisson ratio of the material are in listed Fig. 3. The true strain-stress data used in ABAQUS is transformed from the engineering stress-strain curves of Fig. 3.

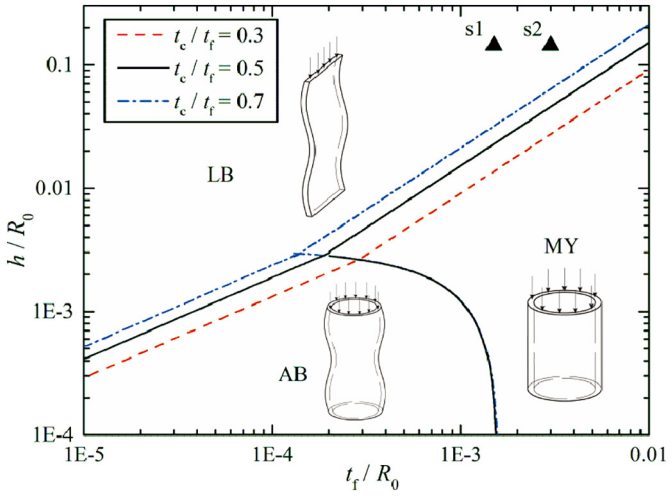

Fig. 5. The initial failure map for corrugated-core sandwich cylindrical shells.

5. Results and discussion

In this section, axial compressive responses of corrugated-core sandwich cylindrical shell obtained from experiments, simulations and theoretical analysis are presented and discussed. Additionally, parameters studies based on FE simulations and theoretical analysis are performed in terms of compressive initial failure load. Subsequently, minimum weight design is carried out for both sandwich cylindrical shell and monolithic cylindrical shell. Finally, a strengthening method is proposed.

5.1. Results of experiments and numerical simulations

5.1.1. Comparison between experimental and simulated results

Fig. 6 presents typical mechanical response curves for S1 and S2, with representative deformation configurations for S2 displayed in Fig. 7. Cross-sectional views of the sandwich cylindrical shell when compressed to 35% and 75% are presented in Fig. 8. In general, in Fig. 6, the simulated load versus displacement curves compare quite well with the measured curves. However, some discrepancies do exist. The difference in strength is mainly attributed to the defects induced during fabrication, especially during the process of stamping and shape correction. Some of the core webs may be somewhat curved because of the error resulted from the springback. Moreover, the thickness of the adhesive may be uneven in some bonding area, and the peeling of adhesive between the core and facesheets (debonding, as shown in Fig. 7) may occur during the folding deformation. The latter is attributed to the fact that local depressions in adjacent core units combine to form a whole depression, leading to the error in plateau stress.

Fig. 7 displays the experimentally observed deformation modes of S2 corresponding to the numbered bullet markers on the measured load versus displacement curve of Fig. 6b. The load versus displacement curve exhibits an initial linear regime, followed by a peak load at point 1. At this point, local depression, as shown in Fig. 7, occurs within the bonding areas of core webs, indicating the formation of the first plastic hinge. After the peak load, there is a sudden drop in the curve as the

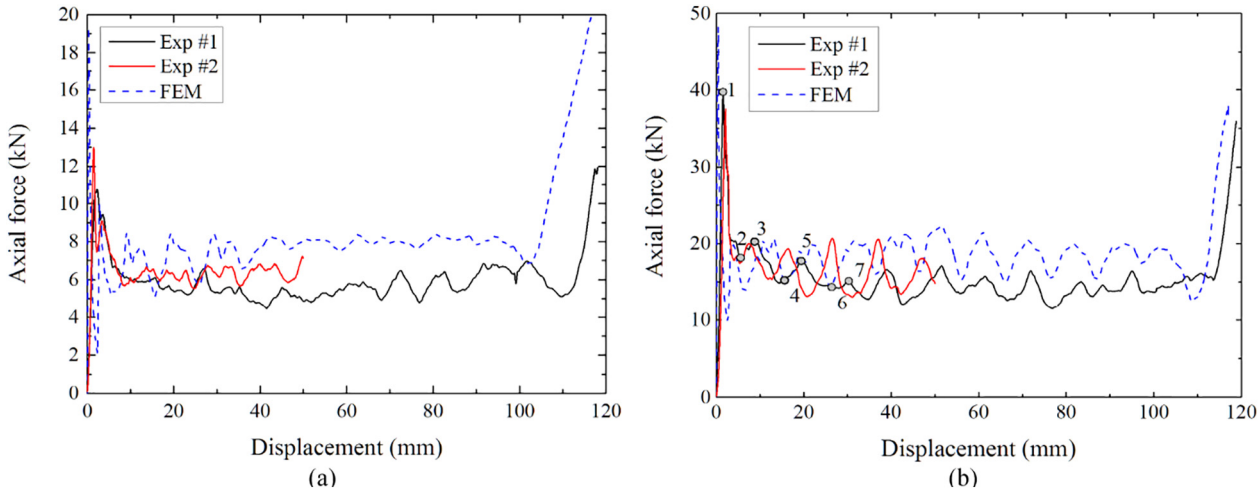

Fig. 6. Load versus deflection curve of corrugated sandwich cylindrical shell for specimen: (a) S1 (#1 and #2) and (b) S2 (#1 and #2).

local depression expands. With further compression, the initial fold forms along the plastic hinge and finally completes at point 3, corresponding to a sharp rise in load during this process. After point 3, new local depression begins to form and similar deformation process is observed, with alternate appearance of peak and valley in the load versus displacement curve.

Fig. 8 shows the cross-sectional view of the deformation configurations of S1 and S2 at the compression ratio of 30% and 75%, respectively. While the numerically simulated deformation configurations compare well with those captured from the experiments, the comparison is better for S2 than S1. This is because that the defects induced by the fabrication process (in particular, stamping and shape correction) in

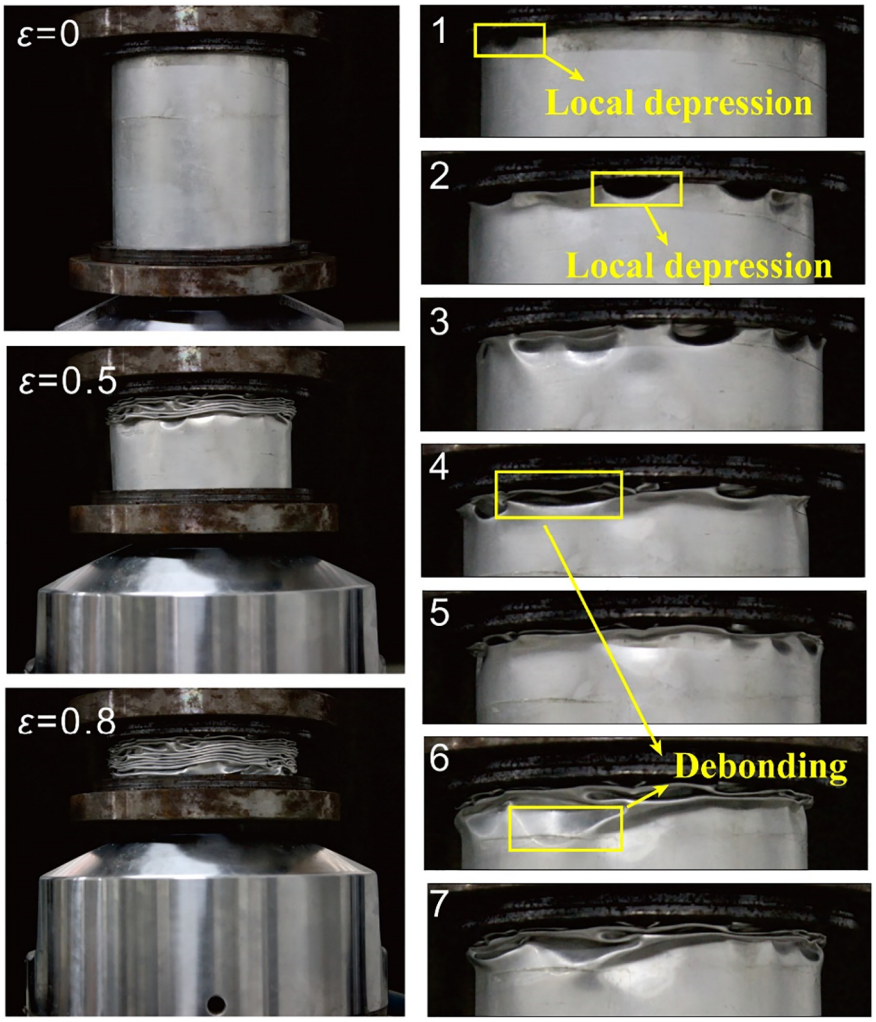

Fig. 7. Representative deformation configurations for S2 (#1) during compression, with the strain and labels corresponding to those marked in the load versus deflection curve of Fig. 6(b).

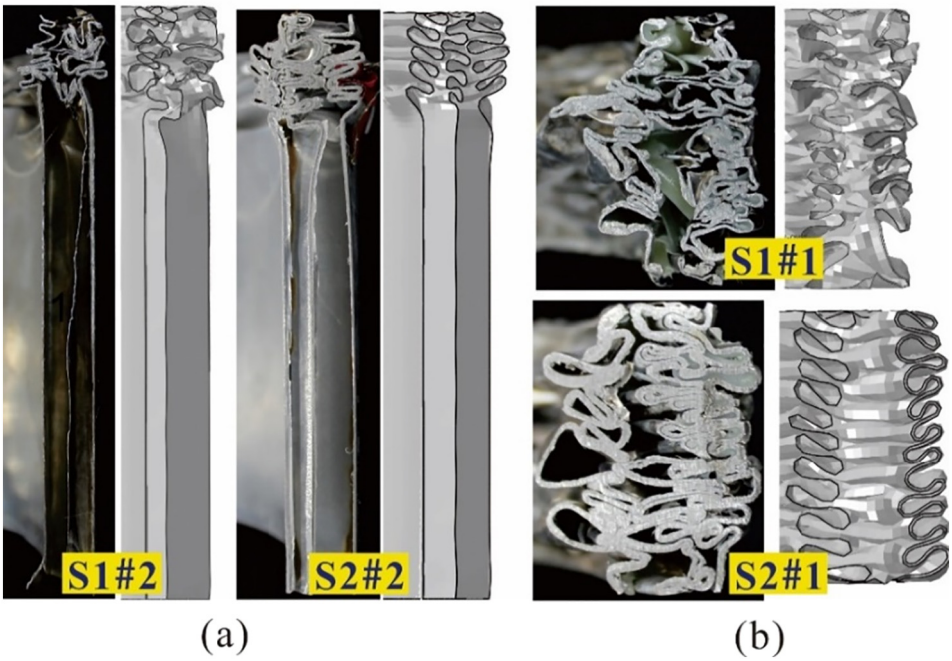

Fig. 8. Cross-sectional views of sample 1 and sample 2 at the compression ratio of (a) 30% and (b) 75%, respectively. For each pair, the left one is experimental diagram and the other is the simulated diagram.

relatively thick samples are less than those in the thinner ones. Interaction effects between the corrugated core and facesheets (both inner and outer) can be found from the same number of folds in core webs and facesheets and the interactive folding of core webs and facesheets.

5.1.2. Initial collapse and crushing response

In this section, the detailed initial collapse and crushing response of the sandwich cylindrical shells are presented with simulated results (only S2 presented for brevity). The force-displacement response of the sandwich cylindrical shell is shown in Fig. 9. The initial collapse includes the initial elastic failure and final failure. While the complex plastic deformation mainly including the formation and expand of the folds following the initial collapse is discussed in the crushing stage. For clearer observation of the deformation corrugated cores, only a unit cell of the core is presented in the simulated results although we carried out the simulation for the entire structure.

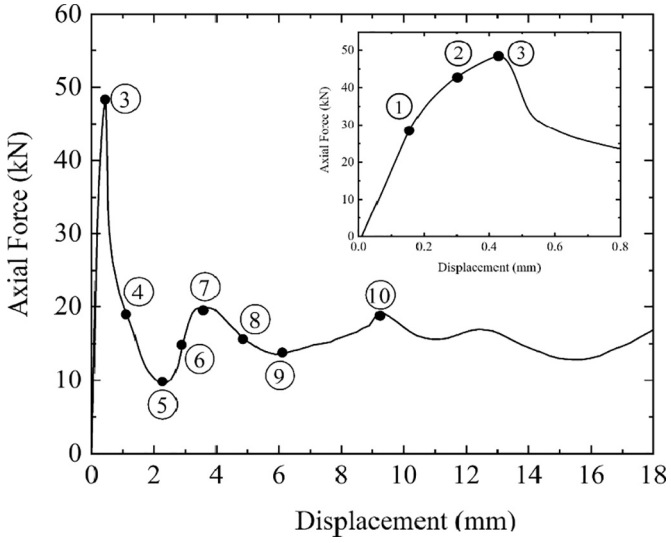

Fig. 9. Simulated force-displacement response of initial collapse and crushing behavior of the sandwich cylindrical shell.

The initial collapse response starts with the origin of the coordinate and ends with point 3 in Fig. 9. Representative contours of the von Mises stress and displacement (perpendicular to the corrugated core web) corresponding to the numbered bullet markers on the response curve are displayed in Fig. 10. Upon compression, the force versus displacement curve exhibits no meaningful deviation from the linear behavior until point 1. As the force approaches this value, lateral deflection of the corrugated core web increases dramatically (Fig. 10, configuration 1) and local buckling occurs (in fact, as configuration 1 exceeds the rear local buckling point due to the output accuracy in simulations, the method for the exact determination of local buckling load is described in the next section). Configuration 1 represents a typical buckling behavior, which is defined as local buckling in this work. It should be noticed that the facesheets remain still in the elastic regime expect for both of the ends that are influenced by boundary effects. Subsequently, the curve enters a nonlinear region from point 1 to point 2. The plastic regime of the core expands and the facesheets yields (configuration 2). With further compression, the peak force is reached at point 3, followed by a sudden drop due to significant deformation of the facesheets and core (configuration 3). In passing, we notice that the initial collapse response of the proposed sandwich structure is complicated. The facesheets are still in elastic regime while the core fails in local buckling. Further, yielding of the facesheets and post buckling of the core develop simultaneously. Indeed we find it difficult to construct a theoretical model for the non-linear regime (post buckling) in the initial collapse response of the sandwich structure.

Following the initial collapse (configuration 3), the folding deformation dominates with further compression. The folding area with two different views, corresponding to the numbered bullet markers on the response curve of Fig. 9, are displayed in Fig. 11. For a clearer observation of the crushing response, different colors are adopted to represent the three main constituents of the sandwich-walled shell: red for the outer-facesheet, green for the corrugated core, and white for the inner-facesheet. With further compression, the first fold starts to form (configuration 4), accompanied by the downward trend in the response curve. The downward trend ends at point 5, wherein the contact of the outer-facesheet and the corrugated occurs for the first time, named here

as I contact (configuration 5). Subsequently, the second contact (II contact) zone emerges during point 5–7 so that the curve exhibits the upward trend. The upward trend remains till configuration 7, at which point a new fold is initiated. When configuration 9 corresponding to the force valley in the load-force curve of Fig. 9 is approached, the third contact (III contact) zone emerges, causing another upward trend of the curve till configuration 10. It is interesting to observe that the fold formed in the corrugated core is embedded in the fold formed in the facesheets. In other words, as the facesheets and core are perfectly bonded at the platform, they fold together and intrude into each other.

For comparison, the axial compressive performances of monolithic cylindrical shells are also studied by FE simulations. For the simulations, two samples with identical mass as sandwich S1 and S2, named below as Tube T1 and Tube T2, are considered. The radius of T1 and T2 is taken as $(R_o + R_i)/2$. For the two groups, the energy absorption of sandwich shells is increased by 37% and 46% than that of the monolithic shell when compressed to densification. The force-displacement curve for the monolithic shell is not shown for brevity. The increment in energy absorption is mainly attribute to the coupling effect of sandwich core and facesheets, which is explained with an entire structure when compressed to densification (Fig. 12a) and partial structure when compressed to 45% (Fig. 12b).

In the view of the entire collapsed structure, axisymmetric mode and non-symmetric mode occur for T1 and T2, respectively, as shown in Fig. 12a. For corrugated-core sandwich cylindrical shells, due to the coupling effect, an axisymmetric collapse exists in overall deformation, and the folding deformation expands to several sub-folds along the ring direction (Fig. 12a), which may be referred to as the "*localized axisymmetric folding mode*". Besides, the number of lobes on the wall increases from 15 to 21 for both S1 and S2. The extended sub-folds and increased lobe numbers both lead to larger region of plastic deformation.

From the partial view shown in Fig. 12b, the coupling effect can be explained in a clearer way in two aspects. First, when compressed to the same distance, the plastic folding deformation forms 11 lobes on the sandwich wall, which is more than the 8 lobes formed in the monolithic shell. Second, in a single fold, the plastic zone in the monolithic shell is only concentrated in the circular plastic hinge line. However, in the sandwich-walled shell, the facesheets and the corrugated core fold together and intrude into each other, which further improve the energy absorption of the proposed structure.

As a result, the energy absorption capacity of the sandwich cylindrical shell is superior to the monolithic one.

5.2. Comparison with theoretical analysis

Table 2 compares the failure loads derived from experiments, analytical predictions and simulations, with both initial failure load and finial failure load considered. The initial failure load indicates the limit of elastic regime, while the failure load is defined as the maximum load on the load versus deflection curve. The initial failure load is difficult to define in experiments due to fabrication induced defects in test samples. As a result, the initial failure load is only presented with analytical prediction and FE simulations. The final failure load is presented with both simulations and experiments, because the process of failure beyond the elastic regime is difficult to obtain with the analytical method.

With reference to Fig. 13, the numerically simulated axial force versus maximal deflection perpendicular to corrugation webs are obtained, and a 6th order polynomial is employed to fit the simulated data (solid red line). Local buckling point is determined by the inflection point of the fitted curve, which can be obtained by finding the minimal root of the second derivative of the polynomial, as detailed in Refs [23,24]. In theoretical analysis, initial failure is dominated by the mode with the lowest failure load. For S1 and S2, local buckling occurs with the lowest load and the failure loads are consistent with the simulated results. The experimentally measured loads are less than those of simulations, due to defects in fabrication and peeling of adhesive surface during compression. To avoid such debonding of adhesive interfaces, better fabrication methods such as cold squeezing, will be developed in future work.

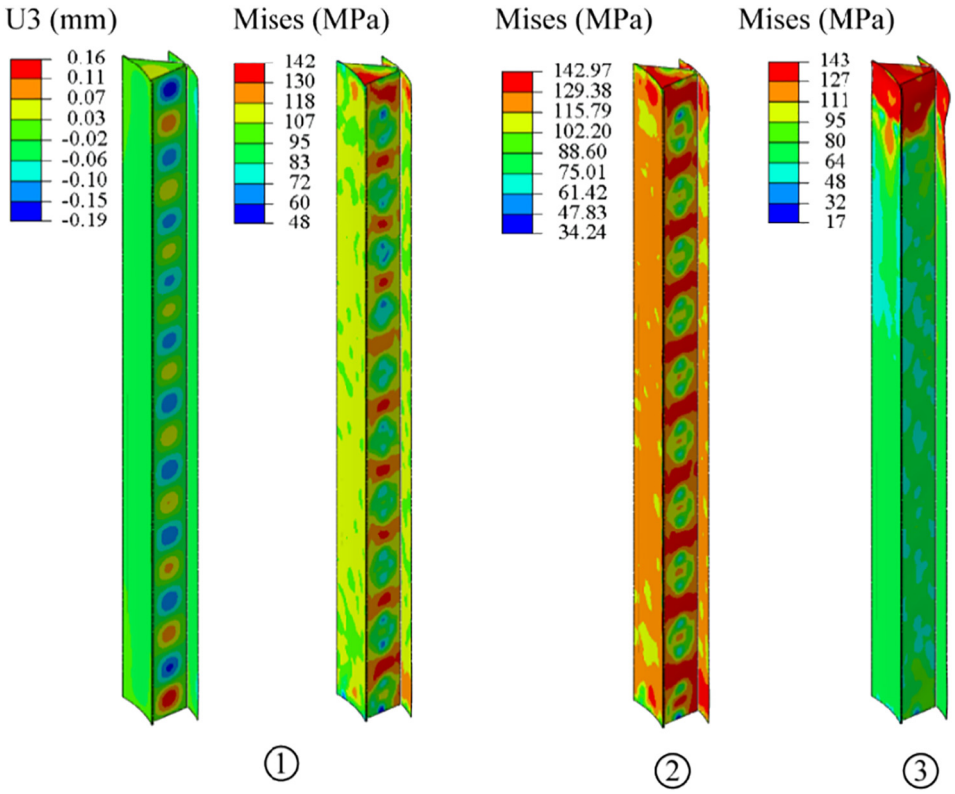

Fig. 10. The initial collapse response of the corrugated core and final failure of the sandwich cylindrical shells.

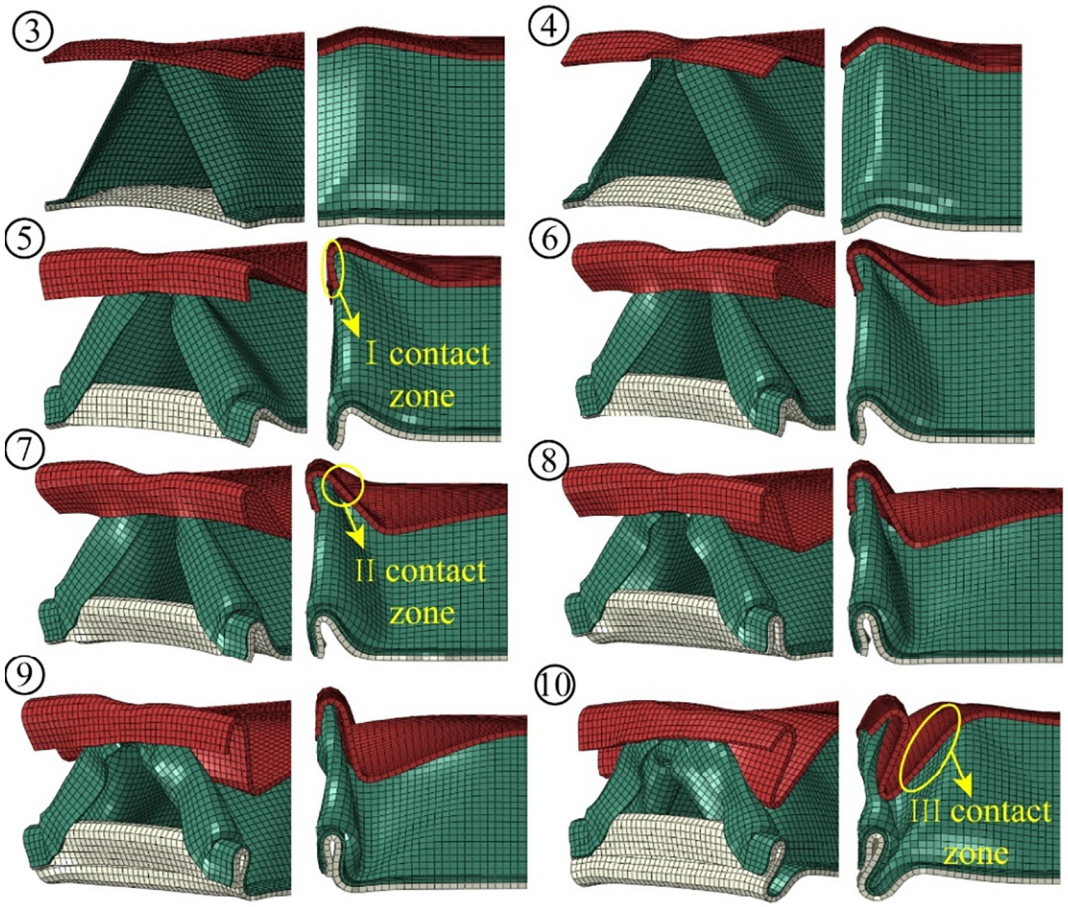

Fig. 11. Deformation configurations with two different views at various stages of crushing corresponding to the numbered bullets marked on the force versus displacement curve of Fig. 9.

5.3. Effect of geometric parameters

The roles played by geometric parameters in the initial failure load of corrugated-core sandwich cylindrical shells are studied with FE simulation and theoretical analysis, as shown in Fig. 14. The ratio of core web thickness to facesheet thickness (t_c/t_f), the ratio of core height to radius of cylindrical shell (h_c/R_o), and the number of corrugated units in the core (N) are taken into account. It should be noticed that, although the above non-dimensional parameters are varied during the analysis, the mass of the sandwich shells remains constant. Neither Euler buckling nor axisymmetric buckling occurs in this study and thus are both neglected in Fig. 14. As can be seen in Fig. 14, the failure loads obtained from analytical predictions for either local buckling or material yielding compare well with those calculated numerically.

As shown in Fig. 14a–c, when N increases, the failure load of local buckling increases. While for the sandwich cylindrical shells discussed in Fig. 14d, the failure load of local buckling first increases, then remains constant as N increases. However, the failure load of material yielding

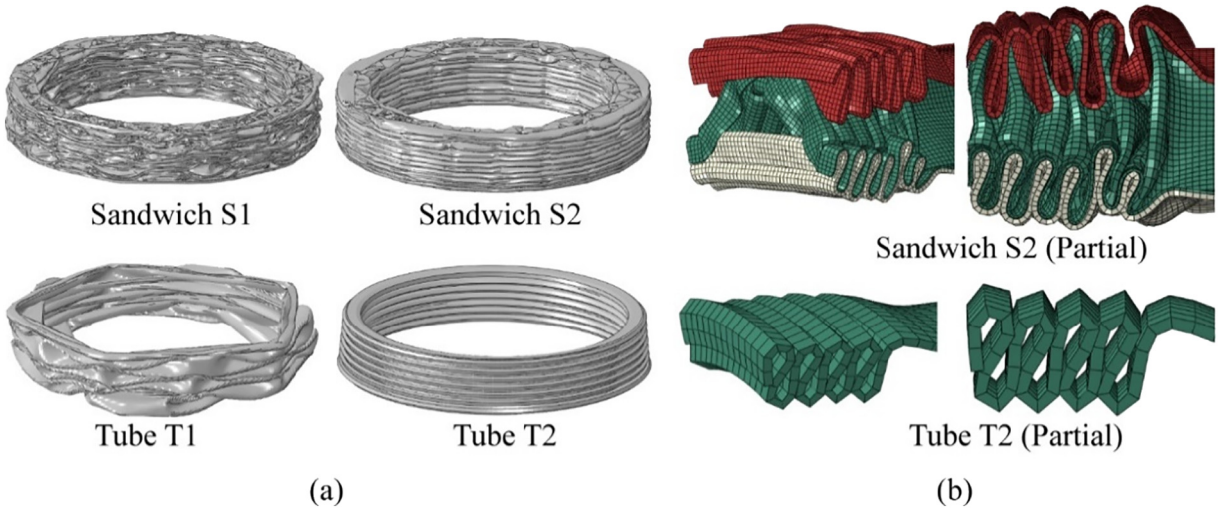

Fig. 12. Collapse configurations for (a) entire view of S1, S2, T1 and T2 when compressed to densification. (b) Partial view of S2 and T2 with compression ratio of 45%.

Table 2
Failure loads of fabricated samples and finite element supplements.

Specimen	Analytical modes/loads (kN)	FE simulations modes/loads (kN)	Experiments load (kN)
S1	LB/3.5	Initial: LB/4.6 Final: 19.6	12.96(#1) 10.92(#2)
S2	LB/28.3	Initial: LB/31.7 Final: 48.3	40.1(#1) 37.02(#2)

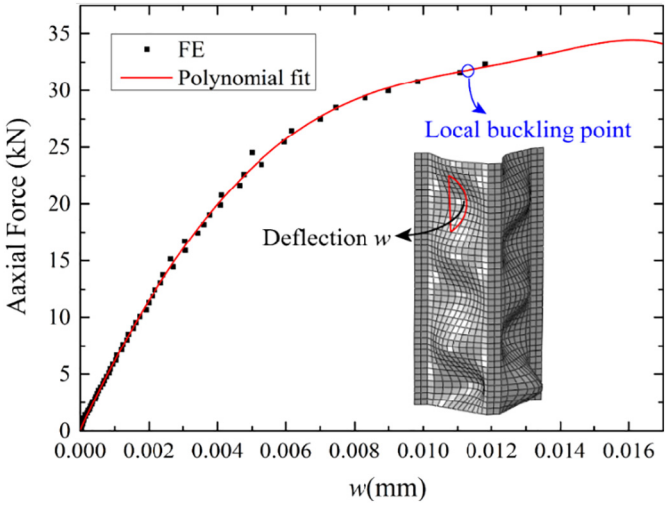

Fig. 13. Numerically simulated axial force versus maximal deflection perpendicular to corrugation webs for S2.

remains constant when N increases. It has been established that for the given t_c/t_f and h_c/R_o, there is a transformation from local buckling to material yielding as N is increased in all sandwich shells, expect for the case of $t_c/t_f = 0.5$ and $h_c/R_o = 0.14$.

It is found that, for a given value of t_c/t_f, the sandwich shells mainly fail in local buckling when the value of h_c/R_o is increased; while for a given value of h_c/R_o, the sandwich shells mainly fail in local buckling when the value of t_c/t_f is decreased. In other words, local buckling dominates in shells with larger h_c/R_o and smaller t_c/t_f.

Meanwhile, a parametric study of the energy absorption capacity of the proposed sandwich cylindrical shell is carried out with FE simulation. To this end, the number of corrugated units N as well as t_c/t_f and h_c/R_o are taken into consideration. As shown in Fig. 15, for all the sandwich cylinders considered, when N is increased, the energy absorption increases. In general, sandwich cylinders with $t_c/t_f = 1$ have better energy absorption capacity than those with $t_c/t_f = 0.5$. For the case of $t_c/t_f = 1$, sandwich cylinders with $h_c/R_o = 0.15$ perform better when N is less than 20. However, when N exceeds 20, sandwich cylinders with $h_c/R_o = 0.1$ have better energy absorption capacity instead. Sandwich cylinders with exhibit similar behaviors. Sandwich cylinders with $h_c/R_o = 0.15$ absorb more energy when N is less than 25 but the trend is reversed if N exceeds 25.

In Fig. 15, the energy absorption capacity of a monolithic cylindrical shell with equal mass to the sandwich shell is presented for comparison. The right axis of Fig. 15 indicates the ratio of energy absorption of sandwich cylinder versus monolithic shell, represented by $E_{sandwich}/E_{monolithic}$. When the value of N exceeds 15, all the sandwich structures have superiority in energy absorption and the advantage increases with increasing N. For instance,$E_{sandwich}/E_{monolithic}$ reaches 2.3 when N is 35, suggesting that the proposed sandwich-walled shell structures have significant advantages over monolithic cylindrical shells having equal mass.

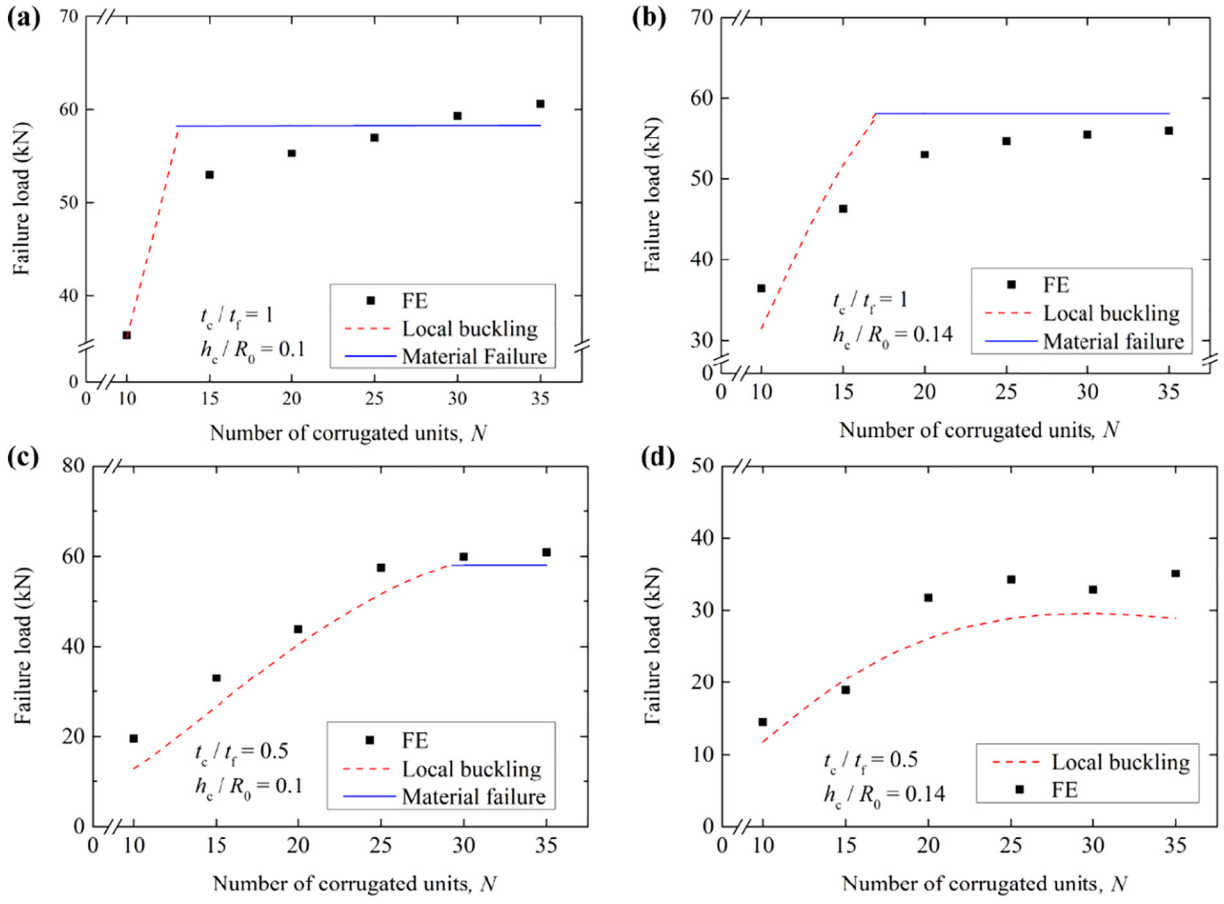

Fig. 14. Parameters study with selected values of t_c/t_f and h_c/R_o: (a) $t_c/t_f = 1$ and $h_c/R_o = 0.1$; (b) and $h_c/R_o = 0.14$; (c) $t_c/t_f = 0.5$ and; (d) $t_c/t_f = 0.5$ and $h_c/R_o = 0.14$.

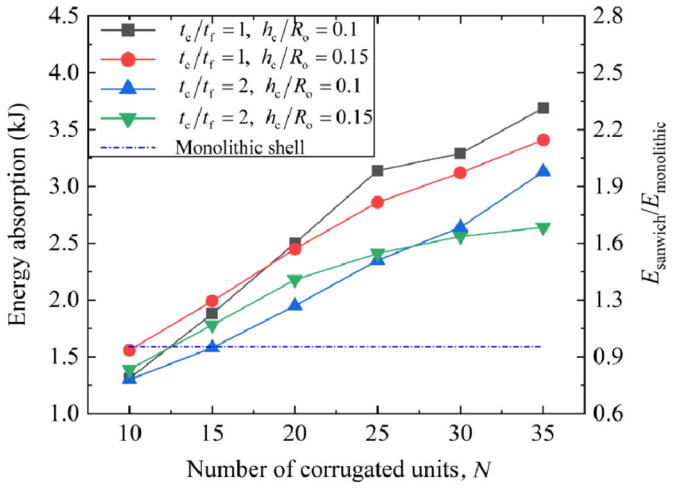

Fig. 15. Energy absorption capacity plotted as a function of the number of corrugated units N for selected values of t_c/t_f and h_c/R_o.

5.4. Minimum weight design

Based on the sequential quadratic programming (SQP) algorithm coded in MATLAB, the minimum weight design under the given axial compression loads is carried out for sandwich cylindrical shell with corrugated core as well as monolithic cylindrical shell for comparison. The design constraint is that none of the failure modes detailed in Section 3.1 (sandwich cylinder) and Appendix A (monolithic cylindrical shell) occurs. This means the failure loads of all failure modes in the optimized structure should be less than the specific $\overline{P}$.

For the sandwich cylindrical shell, the non-dimensional geometric parameters, $\bar{t}_f = t_f/R_o$, $\bar{t}_c = t_c/t_f$, $\bar{h} = h/R_o$, $\bar{L} = L/R_o$ as well as the angle of corrugation α are selected as the design variables, subjected to the limits of $5E\text{-}4 \le \bar{t}_f \le 0.05$, $0.01 \le \bar{t}_c \le 1$, $0.01 \le \bar{h} \le 0.3$, $1 \le \bar{L} \le 10$ and $0.34 \le \alpha \le 1.22$ for practical engineering application and fabrication. The corresponding non-dimensional mass per length $\overline{W}$ and axial compression load $\overline{P}$ can be defined as:

$$\overline{W} = \frac{W}{\rho R_o^2} \tag{10}$$

$$\overline{P} = \frac{P}{E R_o^2} \tag{11}$$

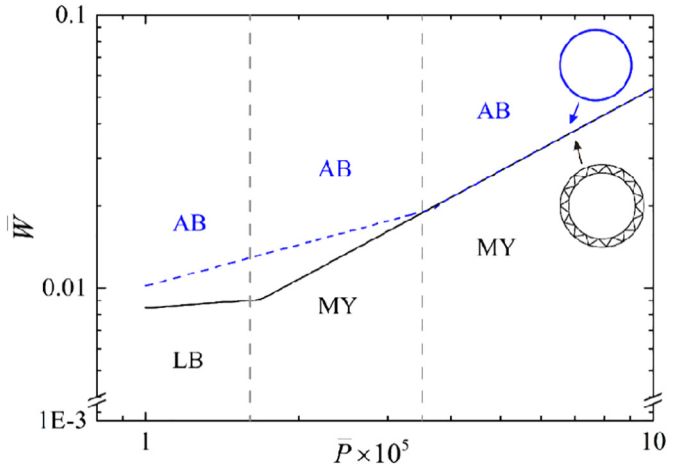

Fig. 16. The minimum weight $\overline{W}$ for corrugated-core sandwich cylindrical shell and monolithic cylindrical shell plotted as functions of axial compression load $\overline{P}$.

For the monolithic cylindrical shell, the non-dimensional geometric parameters, $\bar{t} = t/R$, $\bar{L} = L/R$ are adopted to carry out the minimum weight design, where t, R, L represent the thickness, radius and height of the shell. The limits are given as: $5E\text{-}4 \le \bar{t} \le 0.05$, $1 \le \bar{L} \le 10$. Euler buckling, axisymmetric buckling and material yielding are taken into consideration. The correspondingly failure loads and mass per length of the monolithic shell are presented in Appendix A.

The minimum mass $\overline{W}$ for sandwich shell and monolithic shell as functions of axial compression load $\overline{P}$ are compared in Fig. 16. According to the failure modes, the curves in Fig. 16 can be divided into three parts. In the first part (I), the sandwich shell fails in local buckling while the monolithic shell fails in axisymmetric buckling. It can be found that the superiority of sandwich shell over monolithic shell increases with the increasing value of axial compression load, with the maximum weight deduction increased by 32% for the sandwich shell relative to the monolithic shell. As for the second part (II), the monolithic shell still fails in axisymmetric buckling but the failure mode of sandwich cylindrical shell is transformed into material yielding. Consequently, the superiority of sandwich shell over monolithic shell still exists, although decreasing with increasing axial compression load. Ultimately, both the sandwich shell and the monolithic shell fail in material yielding with equal load-carrying ability as the axial compression load increases further, as seen in the third part (III).

5.5. Strengthening of corrugated-core sandwich cylindrical shell

In recent years, the concept of foam/honeycomb filling in corrugated-core sandwich structures has been proposed to enhance further the strength and energy absorption ability of such structures [36–39]. To identify whether foam filling could increase the strength and energy absorption ability of the present corrugated-core sandwich cylindrical shell, a tentative experimental study of axial compression of foam-filled corrugated-core sandwich cylindrical shell is conducted.

As shown in Fig. 17, the PMI foam of 52 kg/m^3 is used to fully fill the core interstices of the corrugated-core sandwich cylindrical shell with the E-120HP epoxy adhesive evenly smeared in the outside of the foam. Quasi-static axial compressive test is then carried out. Fig. 12 compares the measured axial force versus displacement curves of the foam cylinder with equal mass to the filling foam (labelled as Foam), empty corrugated-core and foam-filled corrugated-core sandwich cylindrical shells (labelled as Cylinder and Foam filled cylinder, respectively).

It is noticed that the curve "Foam + cylinder" indicates the superposition of curves of foam and empty corrugated-core sandwich cylindrical shell. The shaded area indicates the positive coupling effect induced by the filling foam, which leads to greatly enhanced strength and energy

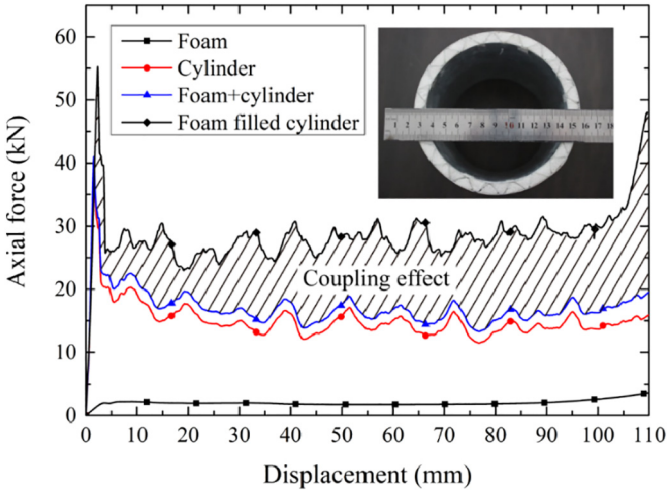

Fig. 17. Experimentally measured axial force versus displacement curves of PMI foam, empty corrugated-core and foam-filled corrugated-core sandwich cylindrical shells.

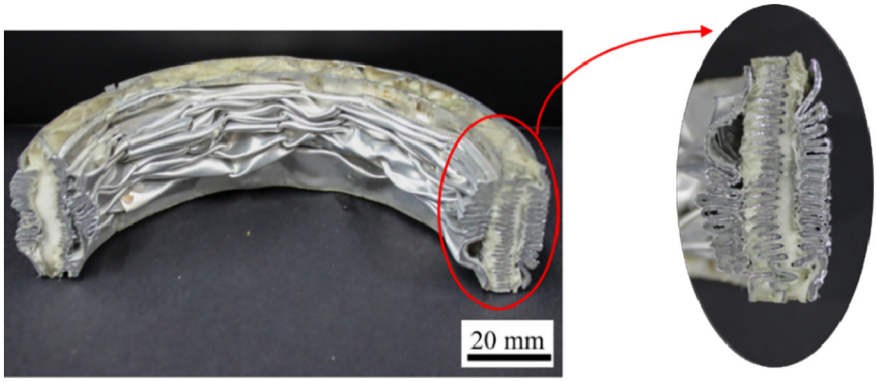

Fig. 18. Cross-section of deformation configuration of foam-filled corrugated-core sandwich cylindrical shell at the compressive strain of 75%.

absorption: 30% and 67% compared with those of the "Foam + cylinder". The coupling effect can be demonstrated from Fig. 17, which presents the radial cross-section of the deformation configuration of the foam-filled sandwich shell at a compressive strain of 75%.

Compared with the cross-section of unfilled sandwich shells as shown in Fig. 8, the coupling effect between the foam and the corrugated-core sandwich shell can be discussed in two different mechanisms of energy dissipation, as described by Santosa [35]. The first mechanism is that the bending and shear loads in the facesheets and the corrugated core are transferred to the foam via the adhesive bonding. In this case, the adhesive layer outside the foam is intact, leading to the high stiffness and initial local buckling load, which can be seen from the force-displacement curve of Fig. 17. Often, such a high crushing force would lead to an extensional folding mode [35]. The second mechanism is the evolution of folding deformation accompanied with the peeling of the adhesive layer. During compression, the adhesive layer is gradually peeled, weakening thus the bond between the foam and metallic wall. As shown in Fig. 18, in the facesheets, the folds outward from the filling foam is free of restriction while the folds inward from the filling foam is prevented by the foam. Different from the facesheets, the walls in the corrugated core are supported by the foam on both sides. As a result, the walls fold together with the filling foam although peeling occurs during the folding deformation. Further, because the facesheets and the corrugated core encroach on the filling foam, the volumetric compressive ratio of the foam filler increases, resulting in enhanced crushing behavior. Also, folding deformation forms 21, 48 and 26 lobes in the inner facesheet, in the corrugated core and in the outer facesheet, respectively, significantly more than that formed in the monolithic shell. The increased number of lobes also greatly enhances the energy absorption capacity of the sandwich-walled shell. Inspired by such strengthening effect, more detailed study based on FEM, experiments and theoretical analysis will be developed in a future work.

6. Conclusions

A combined experimental, analytical and numerical approach is employed to investigate the quasi-static axial compressive response of novel all-metallic ultralight corrugated-core sandwich cylindrical shells. The main findings are summarized as follows:

(1) For the configurations considered in the present study, the energy absorption capacity of the proposed sandwich shell is significantly increased relative to monolithic shell with equal mass. The superiority of sandwich shell over monolithic shell in terms of energy absorption can reach over 100% based on simulated results.

(2) In contrast to the monolithic shell, the enhancement in energy absorption is attributed mainly to the coupling effect between facesheets and corrugated cores, which leads to the increased number of lobs formed during folding deformation, mutually intruding lobes in the corrugated core and facesheets, as well as the extended sub-folds along the ring direction in the sandwich shell.

(3) Based on the parametric study for initial failure load, local buckling plays a dominant role in shells with larger h_c/R_o and smaller t_c/t_f.

(4) In terms of initial failure load, the sandwich shell exhibits superiority over the monolithic shell at relatively low load levels. The monolithic shell fails in axisymmetric buckling while the sandwich shell collapses by local buckling and material yielding.

(5) Foam filling greatly enhances the strength and energy absorption of the sandwich shell. It is mainly attributed to the fact that foam filling increases the number of lobs formed during folding deformation and the metal corrugated webs and the face sheets encroach on the foam.

CRediT authorship contribution statement

Peng-Bo Su: Drafting the article, Data analysis and interpretation. **Bin Han:** Critical revision of the article, Design of the work. **Mao Yang:** Fabrication and experiments. **Zi-Han Wei:** Data collection. **Zhen-Yu Zhao:** Data collection. **Qian-Cheng Zhang:** Fabrication and experiments. **Qi Zhang:** Critical revision of the article. **Ke Ke Qin:** Fabrication and experiments. **Tian Jian Lu:** Design of the work, Critical revision of the article.

Acknowledgment

This work was supported by the National Natural Science Foundation of China (11802221, 11472208, and 11472209), the National Key R&D Program of China (2018YFB1106400), the China Postdoctoral Science Foundation (2016M600782), the Postdoctoral Scientific Research Project of Shaanxi Province (2016BSHYDZZ18), Zhejiang Provincial Natural Science Foundation of China (LGG18A020001), Natural Science Basic Research Plan in Shaanxi Province of China (2018JQ1078).

Appendix A. Failure loads of the monolithic cylindrical shell

For monolithic cylindrical shells, the failure loads and mass per axial length are given by:

$$P_{EB} = \frac{k^2\pi^2 EI}{L^2} \tag{A. 1}$$

$$P_{AB} = \frac{2\pi REt^2}{R\sqrt{3(1-\nu^2)}} \tag{A. 2}$$

$$P_{MY} = 2\pi Rt\sigma_Y \tag{A. 3}$$

$$W = 2\pi\rho Rt \tag{A. 4}$$

References

[1] B.L. Agarwal, L.H. Sobel, Weight comparisons of optimized stiffened, unstiffened, and sandwich cylindrical shells, J. Aircr. 14 (14) (2012) 1000–1008.
[2] J. Hutchinson, M. He, Buckling of cylindrical sandwich shells with metal foam cores, Int. J. Solids Struct. 37 (46–47) (2000) 6777–6794.
[3] F.K. Teichmann, C.T. Wang, G. Gerard, Buckling of sandwich cylinders under axial compression, J. Aeronaut. Sci. 18 (6) (1951) 398–406.
[4] B. Budiansky, On the minimum weights of compression structures, Int. J. Solids Struct. 36 (24) (1999) 3677–3708.
[5] E.H. Baker, Experimental investigation of sandwich cylinders and cones subjected to axial compression, AIAA J. 6 (9) (1968) 1769–1770.
[6] C.W. Bert, C.D. Reese, Simplified design equations for buckling of axially compressed sandwich cylinders with orthotropic facings and core, J. Aircr. 6 (6) (1969) 515–519.
[7] C.D. Reese, C.W. Bert, Buckling of orthotropic sandwich cylinders under axial compression and bending, J. Aircr. 11 (4) (1974) 207–212.
[8] R. Tennyson, K. Chan, Buckling of imperfect sandwich cylinders under axial compression, Int. J. Solids Struct. 26 (9) (1990) 1017–1036.
[9] N. Wicks, J.W. Hutchinson, Optimal truss plates, Int. J. Solids Struct. 38 (30−31) (2001) 5165–5183.
[10] L. Valdevit, J.W. Hutchinson, A.G. Evans, Structurally optimized sandwich panels with prismatic cores, Int. J. Solids Struct. 41 (18–19) (2004) 5105–5124.
[11] T. Liu, Z. Deng, T.J. Lu, Design optimization of truss-cored sandwiches with homogenization, Int. J. Solids Struct. 43 (25–26) (2006) 7891–7918.
[12] T. Liu, Z. Deng, T.J. Lu, Bi-functional optimization of actively cooled, pressurized hollow sandwich cylinders with prismatic cores, J. Mech. Phys. Solids 55 (12) (2007) 2565–2602.
[13] Z. Zhang, Y. Li, H. Wu, D. Chen, J. Yang, H. Wu, S. Jiang, G. Chai, Viscoelastic bistable behaviour of antisymmetric laminated composite shells with time-temperature dependent properties, Thin-Walled Struct. 122 (2018) 403–415.
[14] H. Jiang, L. Liang, Y. Xiao, J. Chen, Y. Xu, X. Wang, Three-dimensional transient thermodynamic analysis of laser surface treatment for a fiber laminated plate with a coating layer, Int. J. Heat Mass Transf. 118 (2018) 671–685.
[15] B.P. Russell, V. Deshpande, H.N.G. Wadley, Quasistatic deformation and failure modes of composite square honeycombs, J. Mech. Mater. Struct. 3 (7) (2008) 1315–1340.
[16] M. Karahan, H. Gül, J. Ivens, N. Karahan, Low velocity impact characteristics of 3D integrated core sandwich composites, Text. Res. J. 82 (9) (2012) 945–962.
[17] J.S. Yang, L. Ma, R. Schmidt, G. Qi, K.U. Schröder, J. Xiong, L.Z. Wu, Hybrid lightweight composite pyramidal truss sandwich panels with high damping and stiffness efficiency, Compos. Struct. 148 (2016) 85–96.
[18] F. Yang, S. Cheng, T. Zeng, Z.H. Wang, G.D. Xu, J. Zhai, D.N. Fang, Mechanical and oxidation properties of C/SiC corrugated lattice core composite sandwich panels, Compos. Struct. 158 (2016) 137–143.
[19] J. Xiong, R. Ghosh, L. Ma, A. Vaziri, Y. Wang, L. Wu, Sandwich-walled cylindrical shells with lightweight metallic lattice truss cores and carbon fiber-reinforced composite face sheets, Compos. PART A-Appls. S. 56 (2014) 226–238.
[20] J. Xiong, L. Feng, R. Ghosh, H. Wu, L. Wu, L. Ma, A. Vaziri, Fabrication and mechanical behavior of carbon fiber composite sandwich cylindrical shells with corrugated cores, Compos. Struct. 156 (2015) 307–319.
[21] W. Li, F. Sun, W. Wei, D. Liu, X. Zhang, M. Li, H. Fan, Fabrication and testing of composite corrugated-core sandwich cylinder, Compos. Sci. Technol. 156 (2018) 127–135.
[22] J. Yang, J. Xiong, L. Ma, L. Feng, S. Wang, L. Wu, Modal response of all-composite corrugated sandwich cylindrical shells, Compos. Sci. Technol. 115 (2015) 9–20.
[23] J. Yang, J. Xiong, L. Ma, G. Zhang, X. Wang, L. Wu, Study on vibration damping of composite sandwich cylindrical shell with pyramidal truss-like cores, Compos. Struct. 117 (2014) 362–372.
[24] H.L. Fan, D.N. Fang, L.M. Chen, Z. Dai, W. Yang, Manufacturing and testing of a CFRC sandwich cylinder with Kagome cores, Compos. Sci. Technol. 69 (15–16) (2009) 2695–2700.
[25] D.S. Ghahfarokhi, G. Rahimi, An analytical approach for global buckling of composite sandwich cylindrical shells with lattice cores, Int. J. Solids Struct. 146 (2018) 69–79.
[26] L. Chen, J. Zhang, B. Du, H. Zhou, H. Liu, Y. Guo, W. Li, D. Fang, Dynamic crushing behavior and energy absorption of graded lattice cylindrical structure under axial impact load, Thin-Walled Struct. 127 (2018) 333–343.
[27] S. Jiang, F. Sun, H. Fan, Multi-failure theory of composite orthogrid sandwich cylinder, Aerosp. Sci. Technol. 70 (2017) 520–525.
[28] Y. Han, P. Wang, H. Fan, F. Sun, L. Chen, D. Fang, Free vibration of CFRC lattice-core sandwich cylinder with attached mass, Compos. Sci. Technol. 118 (2015) 226–235.
[29] H. Zhang, F. Sun, H. Fan, H. Chen, L. Chen, D. Fang, Free vibration behaviors of carbon fiber reinforced lattice-core sandwich cylinder, Compos. Sci. Technol. 100 (2014) 26–33.
[30] W. Li, F. Sun, P. Wang, H. Fan, D. Fang, A novel carbon fiber reinforced lattice truss sandwich cylinder: fabrication and experiments, Compos. PART A-Appls. S. 81 (2016) 313–322.
[31] Z. Zhang, S. Liu, Z. Tang, Crashworthiness investigation of Kagome honeycomb sandwich cylindrical column under axial crushing loads, Thin-Walled Struct. 48 (1) (2010) 9–18.
[32] Z.H. Zhang, S.T. Liu, Z.L. Tang, Comparisons of honeycomb sandwich and foam-filled cylindrical columns under axial crushing loads, Thin-Walled Struct. 49 (9) (2011) 1071–1079.
[33] W. Liu, Z. Lin, N. Wang, X. Deng, Dynamic performances of thin-walled tubes with star-shaped cross section under axial impact, Thin-Walled Struct. 100 (2016) 25–37.
[34] Timoshenko S.P., Theory of Elastic Stability, by S. Timoshenko, McGraw-Hill Book Company, Incorporated. (1936).
[35] S.P. Santosa, T. Wierzbicki, A.G. Hanssen, M. Langseth, Experimental and numerical studies of foam-filled sections, Int. J. Impact Eng. 24 (5) (2000) 509–534.
[36] B. Han, L.L. Yan, B. Yu, Q.C. Zhang, C.Q. Chen, T.J. Lu, Collapse mechanisms of metallic sandwich structures with aluminum foam-filled corrugated cores, J. Mech. Mater. Struct. 9 (4) (2014) 397–425.
[37] B. Han, K. Qin, B. Yu, B. Wang, Q. Zhang, T.J. Lu, Honeycomb–corrugation hybrid as a novel sandwich core for significantly enhanced compressive performance, Mater. Design 93 (2016) 271–282.
[38] B. Han, B. Yu, Y. Xu, C.Q. Chen, Q.C. Zhang, T.J. Lu, Foam filling radically enhances transverse shear response of corrugated sandwich plates, Mater. Design 77 (2015) 132–141.
[39] B. Han, Z.J. Zhang, Q.C. Zhang, Q. Zhang, T.J. Lu, B.H. Lu, Recent advances in hybrid lattice-cored sandwiches for enhanced multifunctional performance, Extrem. Mech. Lett. 10 (2017) 58–69.